Research Article | Vol. 27, No. 3 | 4 Feb 2019 | OPTICS EXPRESS 3324
Optics EXPRESS

Y_2O_3 optical constants between 5 nm and 50 nm

JOSEPH B. MUHLESTEIN,[1,2] BENJAMIN D. SMITH,[1,3] MARGARET MILES,[1] STEPHANIE M. THOMAS,[1,4] ANTHONY WILLEY,[1,5] DAVID D. ALLRED,[1,*] AND R. STEVEN TURLEY[1]

[1]*Department of Physics and Astronomy, Brigham Young University, Provo, UT 84602, USA*
[2]*present address: University of Utah, School of Medicine, Department of Internal Medicine, 30 N 1900 E, Room 4C104, Salt Lake City, UT 84132, USA*
[3]*present address: Department of Physics 4-181 CCIS, University of Alberta, Edmonton T6G 2E1, Alberta, Canada*
[4]*present address: Department of Physics and Astronomy, University of Kentucky, Lexington, KY 40506, USA*
[5]*present address: 19232 15th Ave NE #C1, Shoreline, WA 98155, USA*
[*]*allred@byu.edu*

Abstract: We report optical constants of e-beam evaporated yttrium oxide Y_2O_3 thin films as determined from angle-dependent reflectance measurements at wavelengths from 5 to 50 nm. Samples were measured using synchrotron radiation at the Advanced Light Source. The experimental reflectance data were fit to obtain values for the index of refraction and thin film roughness. We compare our computed constants with those of previous researchers and those computed using the independent atom approximation from the CXRO website. We found that the index of refraction near 36 nm is much lower than previous data from Tomiki as reported by Palik. The real part of the optical constants is about 10% to 15% below CXRO values for wavelengths between 17 nm and 30 nm. Films were also characterized chemically, structurally, and optically by ellipsometry and atomic force microscopy.

1. Introduction

In 2000 the IMAGE mission carried into space an EUV instrument designed to produce pictures of the earth's magnetosphere over time [1]. The mirrors in this instrument were designed to reflect EUV light at 30.4 nm using light resonantly scattered from singly-ionized helium (He II) trapped in the magnetosphere. An aluminum filter blocked lines above 86 nm, but there were other atomic lines that could interfere with the task of cleanly photographing the Earth's magnetosphere. One of the dominant background lines was from neutral helium (He I) at 58.4 nm. An effort was made to design a dual-function multilayer mirror coating that strongly reduced the reflectance of this line in a way that did not interfere with the mirrors' intended reflectance at 30.4 nm [2]. As part of this effort, Lunt, et al. used a genetic algorithm program to investigate what materials and thicknesses would produce high 30.4 nm reflectance and low 58.4 nm reflectance [3, 4]. The 36% reflectance at 30.4 nm with 0.2% reflectance at 58.4 nm promised by the Lunt calculations would have been better than alternative designs such as the actual mirror fabricated for the IMAGE mission with about 21% reflectance at 30.4 nm and 0.65% reflectance at 58.4 nm [1]. It would have also been superior to designs using a SiC/Si multilayer mirror similar to the design produced by Soufli, et al. [5] or a SiC/Mg multilayer mirror similar to the design produced by Fernández-Peria, et. al [6] which had reflectances of a few percent at both of these wavelengths.

Such multilayer mirrors usually consist of a stack of many identical bilayers. In turn, the bilayers usually consist of a "high" refractive index material and a "low" index material analogous to high-low, dielectric mirrors in the visible or near infrared. Here high/low means the refractive

#341752 https://doi.org/10.1364/OE.27.003324
Journal © 2019 Received 8 Aug 2018; revised 20 Dec 2018; accepted 1 Jan 2019; published 31 Jan 2019

Optics EXPRESS

index varies much/little from that of vacuum. In the extreme ultraviolet and soft x-ray portion of the spectrum, the best high/low materials are usually two elements. Surprisingly, the program picked, instead, as one of the layers in the bilayer multilayer a compound: yttrium oxide (Y_2O_3) [3]. While this material, also termed yttria, is used in thin-film optics in the near IR, optical, and UV range, its utility in the extreme ultraviolet was unknown [7–9]. We fabricated multilayer mirrors containing yttria using the optimized parameters the genetic algorithm provided. None of them had the reflectance or properties calculated from the tabulated optical constants.

This created a dilemma. Were the optical constants in the EUV incorrect or did the optical constants of thin-film yttria differ significantly from those of a bulk crystal? To complicate matters, published optical constants for Y_2O_3 were noticeably higher than those computed employing the *independent atom approximation* (IAA) with the atomic scattering factors of Y and O. This illustrates the need for accurately measured optical constants in compound materials.

The optical constants of a material are represented by its complex index of refraction, n. In the extreme ultraviolet (EUV) and x-ray portions of the electromagnetic spectrum the index is written in terms of δ and β [10]:

$$n = 1 - \delta + i\beta \tag{1}$$

Here $1 - \delta$ and β are the real and imaginary parts, respectively, of the index of refraction as a function of wavelength. In the x-ray portion of the spectrum the real part of the index δ is usually positive. The notation $1 - \delta$ is used to allow easy comparison to vacuum where $\delta = 0$. Both δ and β are small in the x-ray portion of the spectrum but roughly increase as the square of the wavelength. In the x-ray region, the complex indices of compounds can be approximated from a density-weighted sum of δ and β for each of the individual elements. The basic assumption is that condensed matter can be modeled as a collection of noninteracting atoms. This semi-empirical method is the IAA. Henke et al. report that it works well at wavelengths sufficiently far from absorption thresholds [11]: "In the threshold regions, the specific chemical state is important and direct experimental measurements must be made."

The IAA approach is applicable in the extreme ultraviolet, but as the wavelength increases, weakly bound electrons, such as those involved in chemical bonds, become more important in determining optical constants [12]. Sae-Lao and Soufli discussed the presence of band transitions near 100 eV (12.4 nm) in yttrium [13]. Similarly Tomiki reported peaks in yttria reflectance spectra at 36 and 43 nm [14]. The peaks Tomiki reported were not observed in elemental yttrium spectra observed by Sae-Lao. This suggests that the IAA is not valid at the longer wavelengths in yttria reported in this paper because of both of these effects: the perturbations of the upper bands of yttrium and oxygen and absorption due to near-edge fine structure in the vicinity of the N-edges of yttrium.

There has been an increased interest in the optical constants for compounds in the extreme ultraviolet. For example, the optical constants of silicon carbide [15–18], boron carbide [19–21], aluminum nitride [22], silicon monoxide [23] and dioxide [24], zirconium dioxide [25], and various fluorides [26] have been reported in the EUV and VUV. This interest is partly for the materials' use in optical reflectors, either as single-surface or multilayer reflectors. EUV optical constants are also needed for Kramers-Kronig type analyses [19]. In recent years, interest in the use of EUV radiation has intensified in a variety of fields–including producing more powerful computer chips [27], astrophysics, heliophysics [28], and imaging biological systems such as protein structures [29]. These technologies require accurate optical properties in the EUV to advance. As an important example relevant to this work, multilayers containing yttria have been produced and studied as reflectors for the 25 to 35 nm range [30].

Lunt's discovery that an oxide, rather than a pure element, is the preferred "high δ" member of the bilayer pair in the EUV multilayer was novel and invited scrutiny [3]. Thus, determining the optical constants of thin film yttria acquired some importance. Lunt's calculations used data from The Handbook of Optical Constants-Volume 2 [31]. The EUV data therein was extracted

Optics EXPRESS

from figures in Tomiki's 1992 paper on yttria [14]. Tomiki measured the VUV reflectance of single-crystal yttria down to 11.3 nm [9, 14]. Employing a Kramer's-Kronig analysis, they used this data to compute the index of refraction down to 27 nm.

That there is a discrepancy between the various sources is well illustrated by noting similarities and differences in yttria normal incidence reflectance. Our purpose was to investigate the nature of these discrepancies and to extend the range for which the indices of refraction for yttria, particularly in thin film form, are known.

2. Experimental method

2.1. Sample preparation and characterization

Two yttria samples were prepared by electron beam (e-beam) evaporation, each in a different evaporator. The first sample was e-beam evaporated in a diffusion-pumped, glass bell-jar evaporator with a base pressure of about 10^{-6} torr. The 25 mm x 25 mm substrate was held in a planetary stage which rotated during deposition, improving thickness uniformity. Detailed descriptions of how planetary fixtures work to improve uniformity are discussed elsewhere [32,33]. The planetary stage was located approximately 50 cm above a graphite crucible which held analytical grade Y_2O_3 chunks. It rotated about the bell jar's center line (axis of symmetry) during the evaporation. As the fixture revolved, geared teeth rotated the individual substrates on an axis pointing toward the center of the chamber to further improve coating uniformity.

Yttria films evaporated onto room-temperature substrates are porous. Such pores absorb water from the air when removed from vacuum [7, 8]. One can reduce porosity by post-deposition heating in air. This has been observed to decrease porosity from about 29% to about 3% [34]. Alternatively, some researchers deposited the film at elevated temperatures. They found that crystallinity and density improves with higher deposition temperature [7, 35–37]. Finally, others have used ion-beam-assisted deposition to densify films as they are being deposited [38]. We used post-deposition annealing, heating Sample 1 at 900K for 29 hours in air. The yttria film's thickness and the refractive indices between 190 to 1000 nm were determined before and after heating using variable-angle, spectroscopic ellipsometry (J. A. Woollam M-1000). The thickness had decreased by about 30% to 20 nm and the refractive index had increased to a value (1.90) closer to bulk (1.932) at 590 nm [39]. Based on these measurement of refractive index at 590 nm we concluded that the postanneal yttria film was greater than 95% dense. The thickness of the film was also determined to be 20.5 nm as part of fitting the samples' indices of refraction using EUV reflection measured on Beamline 6.3.2 as is discussed in the next section. In determining the EUV indices of refraction, the EUV thickness was used rather than the ellipsometric thickness. The ellipsometer and EUV may measure different areas of the sample. Thicknesses and roughnesses are summarized in Table 1. The film's post-treatment root mean

Table 1. Thickness and roughness of Sample 1 and Sample 2.

	thickness (nm)		thickness (nm)	
	ellipso.	EUV	AFM	EUV
Sample 1	20	20.5	0.64	used AFM
Sample 2	17	16	NA	1.06

square roughness was determined to be 0.64 nm when measured over a 1 μm square grid by atomic force microscopy (AFM) [40]. The AFM power spectral density plot for Sample 1 showed a local maxima at about 95 μm^{-1}. This corresponds to features about 10.5 nm wide. Indeed the AFM photograph in Muhlestein [40] shows a surface composed of grains of this lateral size.

Optics EXPRESS

Other film chemical and physical microstructure is discussed below.

Sample 2 was evaporated in a large, cryopumped, stainless steel "box" coater. The 50 mm x 75 mm sample was attached to a planar holder located approximately 40 cm above the electron-beam source. Rotation was unnecessary; the large crucible-sample distance produced satisfactory uniformity. The thickness variation across the sample was less than 2% as determined by ellipsometry. The chamber base pressure was about 10^{-6} torr, and the deposition began once the chamber was evacuated to below 2×10^{-6} torr. To avoid overheating any spot of charge in electron beam evaporation, the beam is typically rastered; however, in this case rastering was not possible. For this reason, the electron beam was significantly higher than optimal and could not be controlled. The increased current caused incandescent Y_2O_3 particles to fly out of the crucible–some striking the substrate holder. To reduce the number of damaging sparks reaching the substrate, a copper mesh of grid spacing 1.41 x 1.95 mm was placed 3 cm below the sample. This screen prevented most Y_2O_3 sparks from reaching the substrate. Following the initial evaporation, another layer was evaporated on top of the first. This sample was heated in air post-deposition at a temperature of 800 K for 20 hours. Using ellipsometry, we verified that the thickness decreased after annealing. The post-anneal ellipsometric thickness of the Y_2O_3 film was measured to be 17 nm. The average thickness of the yttria layer from fitting EUV measurements was 16 nm with a standard deviation of 1.7 nm, thus close to the ellipsometric mesurement [41]. The weighed mean roughness, which was fit as part of the extraction of EUV reflectance for Sample 1, was 1.06 nm.

The chemical makeup of materials can have considerable impact on their index of refraction. To investigate composition x-ray photelectron spectroscopy was employed. The results showed no evidence of nonstoichiometry. The yttrium XPS peak of other annealed yttria samples was that of oxidized yttrium with no discernable peaks or shoulders indicative of yttrium is an oxidation state other than +3. As Wang, et al. point out, postdeposition annealing temperatures above about 775 K produces stoichiometric films as judged by bandgap [34]. Therefore, based on our ellipsometric measurements we conclude that postanneal samples are sufficiently stoichiometric.

Physical structure can also impact indices. This is true for yttria in both the visible and UV regions [34]. Conceivably, it could be also be important in the EUV. Differences in crystallinity and crystal size might, in principle, explain index of refraction variations from the single crystal yttria index of refraction. To investigate their physical structure, the samples similar to those used in this experiment were analyzed using x-ray diffraction (XRD). X-ray diffraction using Cu K_α showed no peaks not attributable to the substrate. While these results might indicate a lack of crystallinity, it is possible that the films were too thin for crystallinity to be detected by XRD. We subsequently made transmission electron micrograph (TEM) measurements of an as-deposited sample. This also showed no evidence of crystallinity. We therefore concluded that it is possible that the films were too thin for crystallinity to be detected by XRD. We subsequently made transmission electron micrograph (TEM) measurements of an as-deposited sample. These also showed no evidence of crystallinity. We therefore concluded that the samples were amorphous as deposited. Wang reported that even after heating, grain size can be very small [34]. In summary, we conclude that both of the postanneal films are stoichiometric, extremely fine grained or amorphous and greater than 95% dense.

2.2. EUV reflectance measurements

Beamline 6.3.2 at the Advanced Light Source (ALS) at Lawrence Berkeley National Laboratory was used to measure the samples' EUV reflectance. The synchrotron source produces broadband EUV light which is dispersed and filtered in the beamline to achieve a spectral purity, $\Delta\lambda/\lambda$, of 99.75%. The desired wavelength enters the sample chamber where it reflects off the Y_2O_3 surface and then is incident on a silicon PIN diode which measures the intensity of the reflected light. The same detector and filters were used for the measurement of the reflected and unreflected

Optics EXPRESS

beams. Since the reflectance is essentially a ratio of these two measurements, any effects of detector efficiency and acceptance effects was normalized out. The angular resolution was less than 0.05 degrees. The Y_2O_3 surface can be rotated to achieve the desired angle of incidence. The light is mostly s-polarized, with the actual fraction of s- and p-polarization a function of the beam energy as shown in Fig. 1 [42].

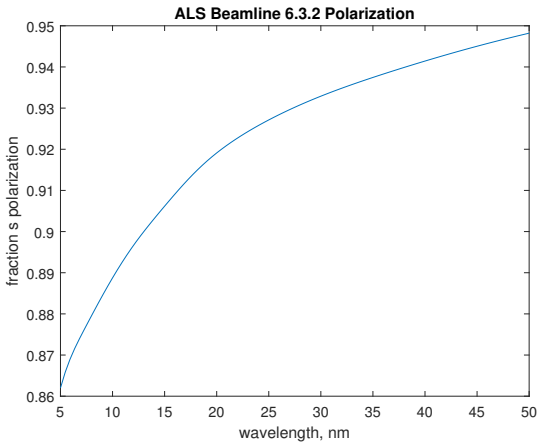

Fig. 1. Polarization of the light in beamline 6.3.2 as a function of wavelength.

In addition to the reflected beam, we also measured the background signal in the detector, I_B. This was done by measuring the signal with the mirror moved out of the path of the beam and the incident beam blocked. Since the background signal depended on the gain G_n of our amplifiers and the measurements were made at a variety of gains, background measurements were made separately for each gain setting. The intensity of the incident beam was also measured directly on the I_0 detector. The synchrotron electron beam current was carefully controlled to <0.1% to keep the light intensity constant.

3. Analysis

The experimental reflectance R_E at each wavelength was calculated as the ratio of the intensity of the reflected beam (I_R) to the intensity of the incident beam (I_0).

$$R_E = \left[\frac{(I_R - I_{B_R})}{G_R}\right]\left[\frac{G_0}{(I_0 - I_{B_0})}\right] \tag{2}$$

The theoretical reflectance for each polarization R_s and R_p were calculated using the Parratt recursion formula [43] relating the ratio of the reflected and incident electric fields. This is discussed further in Johnson's and Muhlestein's theses [40,44].

$$r_{m+1} = C_m^4 \frac{r_m + f_{m,\sigma}}{r_m f_{m,\sigma} + 1} \tag{3}$$

where

$$r_m = C_m^2 \frac{E_m^R}{E_m}, \tag{4}$$

is the ratio of the reflected electric field E_m^R and the incident field E_m half-way between layers m and $m+1$, $f_{m,\sigma}$ is the Fresnel coefficient between layer m and layer $m+1$ for $\sigma = p$ or $\sigma = s$

Optics EXPRESS

polarized light.

$$f_{m,p} = \frac{n_m^2 q_{m+1} - n_{m+1}^2 q_m}{n_m^2 q_{m+1} + n_{m+1}^2 q_m} \tag{5}$$

$$f_{m,s} = \frac{q_{m+1} - q_m}{q_{m+1} + q_m} \tag{6}$$

$$q_m = \sqrt{n_m^2 - \cos^2\theta} \tag{7}$$

$$C_m = e^{ik_m d_m/2} \tag{8}$$

$$k_m = \frac{2\pi n_m}{\lambda} \tag{9}$$

where n_m is the index of refraction in the m^{th} layer and θ is the incident angle measured from grazing. The theoretical reflectance R_T is the weighted sum of the reflected intensities R_s and R_p

$$R_s = |r_s|^2 \tag{10}$$

$$R_p = |r_p|^2 \tag{11}$$

$$R_T = R_s u_s + R_p(1 - u_s) \tag{12}$$

where u_s is the fraction of the incident beam with s polarization.

Along with the Parratt [43] recursion formula, the Debye-Waller [45] correction factor:

$$s = e^{-2q_z^2\sigma^2} \tag{13}$$

was included to account for roughness in the Y_2O_3 layer. The Fresnel coefficient on the top layer was multiplied by s, decreasing the reflectance. Roughness was not included in the lower layers.

The experimental reflectance was fit to the theoretical curve using a weighted least-squares fit that minimized

$$\sum_{i=1}^{N} \left[\frac{R_E - R_T(\theta_i, P_i)}{w_i} \right]^2 \tag{14}$$

where w_i weights the function in such a way that high and low reflectances have roughly equal weight in addition to a constant background error level [46]. N is the total number of data points, θ_i are the incident angles from grazing, and P_i are fit parameters - including the index of refraction n_m and the thicknesses d_m of the film layers. Figure 2 shows four examples of the experimental, grazing-angle reflectance and some of their fits to theoretical reflectance of Sample 1 at 6.5 nm, 12.5 nm, 30 nm and 36 nm. Below 30 nm, β of yttria is sufficiently small that interference fringes can be seen in reflectance graphs of the samples. These peaks and maxima help correctly fit the index of refraction and sample thickness. The poor fit at 12.5 nm is partially due to the challenge of measuring and fitting data at the Si L_3 edge.

4. Results and discussion

Reflectance

The curves in Fig. 3 are from two kinds of near-normal reflectance data: measured sample reflectance and reflectance computed from δ and β. Three measured and one computed (open circle) reflectance curves are shown in Fig. 3. The lower three curves correspond to specularly reflected light incident at 8° from normal. The black diamonds mark reflectance data replotted from Fig. 1 of Tomiki of the near-normal reflectance of the {111} cleaved face of an yttria crystal [14]. Reflectance measured in the present study provide the data marked with the dashed

Optics EXPRESS

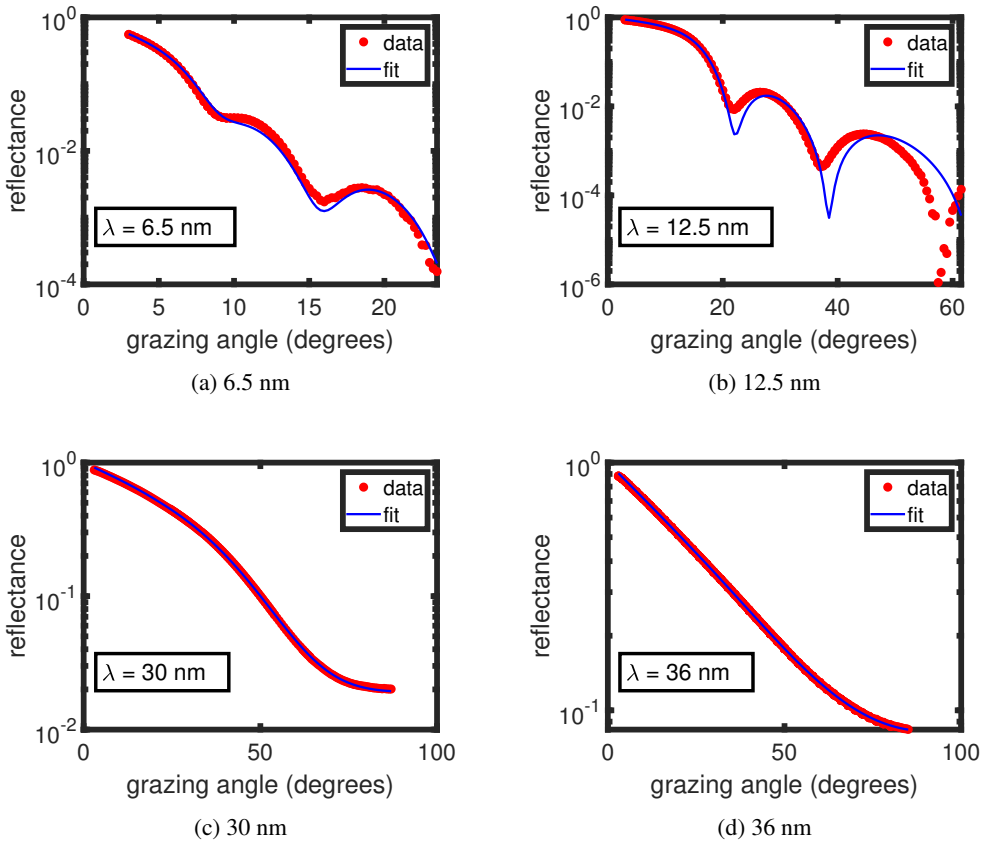

(a) 6.5 nm (b) 12.5 nm

(c) 30 nm (d) 36 nm

Fig. 2. Measured reflectance data (red circles) and fits (solid blue line) for Sample 1 at four wavelengths.

line (Sample 1). The reflectance of optically thick layers can also be computed from δ and β data. The open green circles mark the reflectance calculated via the IAA using Y and O data [10] archived at CXRO, assuming crystal density (5.01 g/cm^3) and no roughness, using the web tool at the site [48].

All of the reflectance curves in Fig. 3 based on yttria *measurements* have a similar form. They have distinct reflectance peaks at approximately 36 and 42.5 nm. In contrast, the reflectance estimated by the IAA with archive data slowly increases with increasing wavelength reaching a single broad maximum at about 38 nm (32.6 eV). In addition, the calculated maximum reflectance is lower than the peaks in Fig. 1 of Tomiki [14] and our Sample 1.

Tomiki identified these peaks as transitions involving electrons leaving the oxygen 2s levels and being excited to empty 4p-4d levels in yttrium. It is noteworthy that the reflectance of both Sample 1 and Kimura's surface have remarkably lower amplitude than Tomiki's crystals [14]. Whereas our samples are thin films, Kimura's and Tomiki, et al.'s are bulk. The bulk samples are the facet of a single crystal. This suggests that the observed reflectance differences between this study and Tomiki's is not due to differences in perfection of the crystals. Likewise crystallographic orientation is not an important factor in EUV reflectance. Kimura's data is an indication that the reflectance measurements reported here are likely valid measurements for yttria over this wavelength range. Furthermore, they are evidence that the handbook constants based on Tomiki's data are incorrect over this range.

Optics EXPRESS

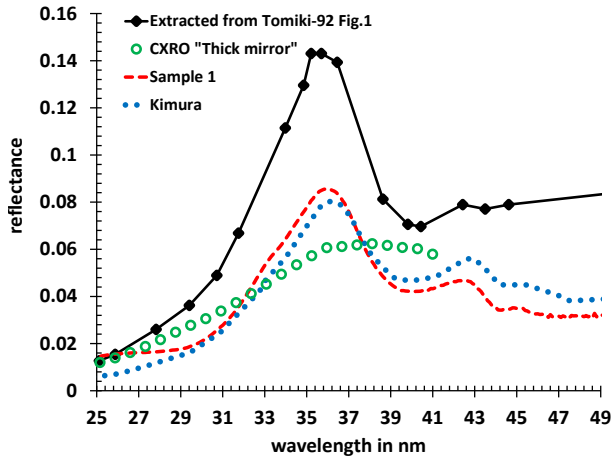

Fig. 3. Near-normal reflectance of a Y_2O_3 surface from various sources. The red dashed line is the measured reflectance of Sample 1. The black diamonds (near top) and the blue dotted line, respectively, mark data extracted from Tomiki's [14] and from Kimura's [47] near-normal reflectance measurements of polished yttria crystals. The large green circles mark the reflectance for 8° from normal incidence calculated for a "bulk-like" sampled, also termed "thick film" via the IAA using Henke's δ and β data for Y and O with no roughness. Kimura's near-normal reflectance measurements of a polished yttria crystal [47] closely matches Sample 1 (of this study). See Data File 1 for underlying values for the reflectance of Sample 1.

It is also noteworthy that IAA calculations for a "thick" yttria mirror yield a smoothly varying reflectance curve that passes through the midpoint of the peaks and valleys seen in Kimura and the present study's reflectances in Fig. 3. The data from Henke [10] are for the Y and O as elements and cannot be expected to show these peaks in the reflectance since they are due to electronic band transitions specific to the oxide. Since the reflectances are small below 31 nm, log of reflectance is replotted for wavelengths between 5 and 31 nm in Fig. 4.

We see that the *calculated* normal-incidence, zero-roughness, thick-mirror reflectances of Sample 1 (triangles) and 2 (filled circles) are similar over most of the range above 19 nm. They lie about 20% below the open green circles which mark the near-normal reflectance calculated via the IAA using the web tool at CXRO [48]. It is noteworthy that below 20 nm the Sample 1 and Sample 2 reflectances diverge. This is where δ and β differ significantly in the two e-beam samples as noted below. Surface roughness was one of the parameters fit in the global fitting of the reflectance of the samples on their substrate. (See Eq. (13).)

Optical constants

In Fig. 5, and Figure 6, δ and β for both Sample 1 and 2 are plotted. For comparison, IAA. Tomiki and Kimura values of delta and beta are also plotted. The most noteworthy features are, first, that the measured delta values are nearly coincident with the IAA data from the CXRO web tool, and second, that in the 30 to 50 nm range, Tomiki and Palik data are distinctly larger than the CXRO and our measured data. On the other hand, beta (Figure 6) deviates significantly from IAA estimates above 30 nm. At 36 nm Sample 1's beta is equal to that by Tomiki. However, for wavelengths above 41 eV Sample 1's beta is significantly lower.

It can be also seen that the measured delta and beta of both samples lie below the IAA values between 17 and 28 nm. However, it is not clear in these figures that they are about 10-15% below the IAA values and that at and below 16 nm the value of delta for Sample 2 coincides with the

Optics EXPRESS

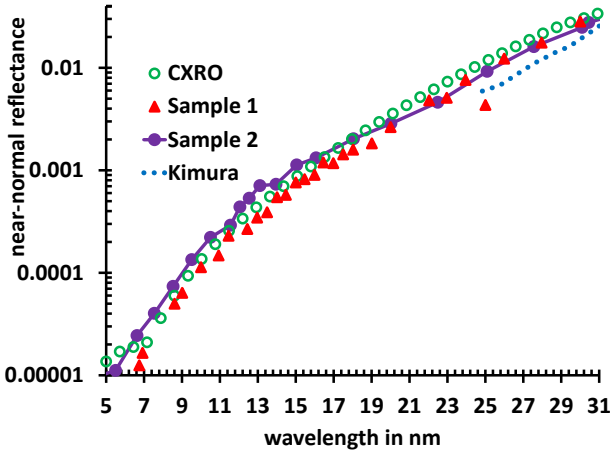

Fig. 4. Measured and calculated, near-normal reflectance of Y_2O_3. The top three entries in the legend are *calculated* from δ and β. The bottom is *measured.* The bottom curve (dotted line) marks the reflectance data extracted from Fig. 1 of Kimura's [47] near-normal reflectance measurements of a polished yttria crystal. The large open green circles mark the reflectance calculated via IAA using the web tool at the CXRO websites for 8° from normal incidence. The filled red triangles and filled purple circles (solid line) respectively correspond to reflectances calculated for a thick mirror at normal incidence based on measurements of δ and β obtained for Sample 1 and Sample 2 in this report.

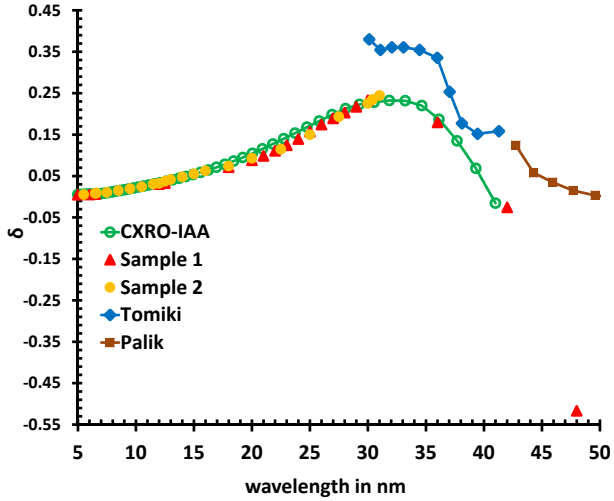

Fig. 5. δ for yttria. The large open circles mark values calculated using the IAA with Henke data archived at CXRO [10]. The solid triangles and circles are the measurements in this study. The filled brown squares are adapted from Tropf and Thomas [31]. As in Figure 3, diamonds denote data from Tomiki et al [14]. See Data File 2 for underlying values of δ for Sample 1 and Data File 3 for underlying values of δ for Sample 2.

IAA, while delta for Sample 1 remains below it. The problem in showing this is that the optical constants δ and β vary by a factor of 40 over this wavelength range and delta and beta values are very small at short wavelengths. This variation is mostly due to δ and β trending with the square of wavelength in the EUV. That is, they are roughly proportional to λ^2. One could replace δ and β for any compound by the factors f_1 and f_2 defined in analogy with atomic scattering factors.

Optics EXPRESS

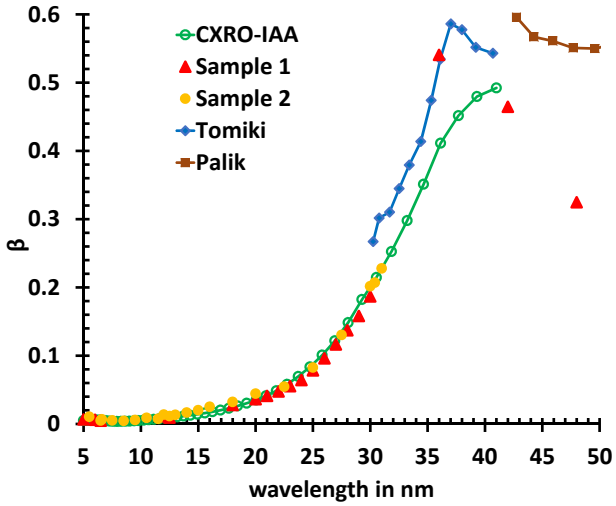

Fig. 6. The imaginary component of the scattering factor β for yttria. The large open circles mark values calculated using the IAA with Y and O data archived at CXRO from [10]. The solid triangles and circles are the measured values in this report for Sample 1 and Sample 2. The blue solid diamonds are derived from Tomiki [14]. The solid brown squares are adapted from Tropf and Thomas [31]. See Data File 2 for underlying values of β for Sample 1 and Data File 3 for underlying values of β for Sample 2.

That is,

$$n = 1 - \delta + i\beta = 1 - \frac{r_0 N}{2\pi}\lambda^2 (f_1 - i f_2) \tag{15}$$

where N is the number of yttrium atoms per unit volume and r_0 is the classical electron radius.

$$r_0 = \alpha \frac{\hbar c}{m_e c^2} = 2.818 \times 10^{-15}\ \text{m}. \tag{16}$$

In such analysis a density is required. We have done such calculations for N using the bulk density for yttria, 5.01 g/cm^3. We show f_1 in Fig. 7. It is clear here that f_1 for sample 1 is about 10-15% below the IAA over the whole range. Similarly, f_1 for sample 2 is also about 10-15% below the IAA from 17 to 35 nm and about the same value elsewhere. Since δ is proportional to f_1 these observations are also true for δ.

In the IAA the interaction of the EUV light with a condensed matter sample is treated as the *sum of the interaction of all the atoms in the material independently.* The index of refraction n for the material is calculated from the individual atomic scattering factors.

$$n = 1 - \delta + i\beta = 1 - \frac{r_0}{2\pi}\lambda^2 \sum_q N_q f^q \tag{17}$$

where N_q is the number of atoms of type q per unit volume, and

$$f^q = f_1 - i f_2 \tag{18}$$

is the scattering factor for atom q. For example, the index of refraction of yttria is

$$n = 1 - \delta + i\beta = 1 - \frac{r_0}{2\pi}\lambda^2 (N_Y f^Y + N_O f^O) \tag{19}$$

Unlike IAA, in our analysis we do not assign the electrons doing the scattering to any particular atom in the molecular unit.

Optics EXPRESS

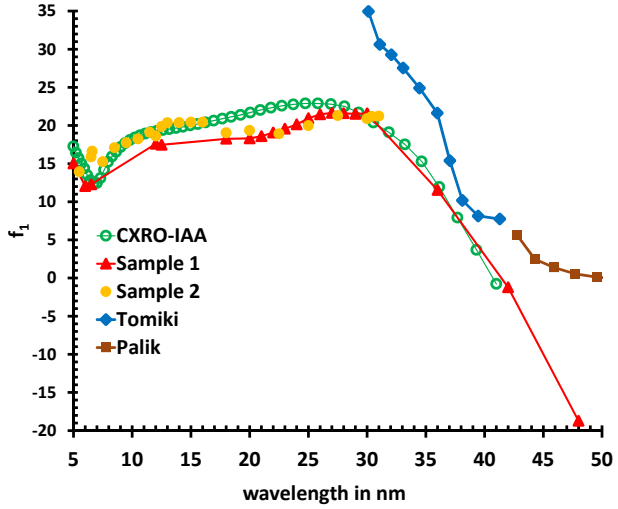

Fig. 7. Real component of the scattering factor, f_1 for yttria. (f_1 is proportional to δ). See Data File 4 for underlying values.

5. Summary and conclusions

The indices of refraction (δ and β) of two yttria samples were experimentally determined for wavelengths of 5–49 nm. The experimentally determined δ and β values from the two samples agree with each other for $\delta > 17$ nm and $\beta > 22$ nm. The measurements from the two samples differ from tabulated values derived by Tomiki, which appear to be too large for $\lambda > 30$ nm. This may account for the inability to accurately simulate multilayer performance for $\lambda > 30$ nm, which uses yttria optical constants from Palik. That Kimura's reflectance data coincides with the present study in amplitude and peak position lends support to the accuracy of the data from this study. It follows that Tomiki's constants are therefore incorrect near the reflectance maxima at 36 nm. Physical structure may not affect δ and β as amorphous or nanocrystalline yttria films possess reflectance values similar to or larger than Kimura measured on single crystals.

The newly determined optical constants will improve EUV multilayer reflector calculations. The computed reflectance at 30.4 nm will be lower than that calculated using previous optical constants.

Funding

Advanced Light Source, a DOE Office of Science User Facility (DE-AC02-05CH11231); Utah Space Grant Consortium (project NASA Grant NNX15AI24H to Margaret Miles and project generally); National Science Foundation (NSF) Directorate for Education and Human Resources (1852152).

Acknowledgments

We gratefully acknowledge the financial support of BYU's College of Physical and Mathematical Science. This material is partially based on work while R. Steven Turley was serving at the National Science Foundation (NSF). Any opinion, findings, and conclusions or recommendations expressed in this material are those of the authors and do not necessarily reflect the views of the National Science Foundation.

We grateful acknowledge Prof. Richard R. Vanfleet for TEM measurements and John E. Ellsworth for aid in the preparation of sample 2 (both of Dept. of Physics and Astronomy, BYU).

Optics EXPRESS

We are also grateful for the assistance of BYU undergraduate students Andrew Jacquire, Zephne Larsen Vaterlaus and Kameron Hansen. We appreciate the assistance of 6.3.2 beamline scientists, Eric M. Gullikson and Andrew Aquila, for aiding us in learning how to take high-quality data on the beamline 6.3.2 system and for many helpful discussions.

References

1. B. Sandel, A. Broadfoot, C. Curtis, R. King, T. Stone, R. Hill, J. Chen, O. Siegmund, R. Raffanti, D. Allred, R. Turley, and D. Gallagher, "The extreme ultraviolet imager investigation for the IMAGE mission," Space Sci. Rev. **91**, 197–242 (2000).
2. D. D. Allred, R. S. Turley, and M. B. Squires, "Dual-function EUV multilayer mirrors for the IMAGE mission," Proc. SPIE **3767**, 280–287 (1999).
3. S. Lunt, "The use of genetic algorithms in multilayer mirror optimization." (Undergraduate Honors Thesis, Brigham Young University, 1999). http://volta.byu.edu/pubs/LuntUGthesis.pdf. Accessed 5 Oct 2016.
4. S. Lunt, R. S. Turley, and D. D. Allred, "Design of bifunctional XUV multilayer mirrors using a genetic algorithm," J. X-Ray Sci. Technol. **9**, 1–11 (2000).
5. R. Soufli, E. Spiller, D. L. Windt, J. C. Robinson, E. M. Gullikson, L. R. de Marcos, M. Fernandez-Perea, S. L. Baker, A. L. Aquila, F. J. Dollar, J. A. Méndez, J. I. Larruquert, L. Golub, and P. Boerner, "In-band and out-of-band reflectance calibrations of the EUV multilayer mirrors of the atmospheric imaging assembly instrument aboard the Solar Dynamics Observatory," in *Space Telescopes and Instrumentation 2012: Ultraviolet to Gamma Ray,* T. Takahashi, S. S. Murray, and J.-W. A. den Herder, eds. (SPIE, 2012), p. 8443C.
6. M. Fernández-Perea, R. Soufli, J. C. Robinson, L. R.-D. Marcos, J. A. Méndez, J. I. Larruquert, and E. M. Gullikson, "Triple-wavelength, narrowband Mg/SiC multilayers with corrosion barriers and high peak reflectance in the 25–80 nm wavelength region," Opt. Express **20**, 24018 (2012).
7. G. Atanassov, R. Thielsch, and D. Popov, "Optical properties of TiO_2, Y_2O_3 and CeO_2 thin films deposited by electron beam evaporation," Thin Solid Films **223**, 288–292 (1993).
8. D. Bezuidenhout and R. Pretorius, "The optical properties of evaporated Y_2O_3-films," Thin Solid Films **139**, 121–132 (1986).
9. T. Tomiki, J. Tamashiro, Y. Tanhara, A. Yamada, H. Fukutani, T. Miayahara, H. Kato, S. Shin, and M. Ishigame, "Optical spectra of Y_2O_3 single crystals in VUV," J. Phys. Soc. Jpn. **55**, 4543–4549 (1986).
10. B. L. Henke, E. M. Gullikson, and J. C. Davis, "X-ray interactions: photoabsorption, scattering, transmission, and reflection at E=50–30000 ev, Z=1–92," At. Data Nucl. Data Tables **54**, 181–342 (1993).
11. B. L. Henke, E. M. Gullikson, and J. C. Davis, "X-ray interactions with matter,," http://henke.lbl.gov/optical_constants/intro.html. (Accessed 17 March 2009).
12. M. B. Squires, R. S. Turley, and D. D. Allred, "Will the real optical constants please stand up: The problem in obtaing optical constants for materials in the VUV," in *Proccedings of the Conference of Physics of X-ray Multilayer Structures,* (1998).
13. B. Sae-Lao and R. Soufli, "Measurements of the refractive index of yttrium in the 50–1300 eV energy region," Appl. Opt. **41**, 7309–7316 (2002).
14. T. Tomiki, T. Shikenbaru, Y. Ganaha, T. Futemma, H. Kato, M. Yuri, H. Fukutani, T. Miyahara, S. Shin, M. Ishigame, and J. Tamashiro, "Optical spectra of Y_2O_3 single crystals in the vacuum ultraviolet region. II," J. Phys. Soc. Jpn. **61**, 2951–2963 (1992).
15. J. I. Larruquert and R. A. M. Keski-Kuha, "Reflectance measurements and optical constants in the extreme ultraviolet for thin films of ion-beam-deposited SiC, Mo, Mg_2Si, and InSb and of evaporated Cr," Appl. Opt. **39**, 2772–2781 (2000).
16. D. Garoli, F. Frassetto, G. Monaco, P. Nicolosi, M.-G. Pelizzo, F. Rigato, V. Rigato, A. Giglia, and S. Nannarone, "Reflectance measurements and optical constants in the extreme ultraviolet-vacuum ultraviolet regions for SiC with a different C/Si ratio," Appl. Opt. **45**, 5642 (2006).
17. M. Fernández-Perea, J. A. Méndez, J. A. Aznárez, and J. I. Larruquert, "In situ reflectance and optical constants of ion-beam-sputtered SiC films in the 58.4 to 149.2 nm region," Appl. Opt. **48**, 4698–4702 (2009).
18. J. I. Larruquert, A. P. Pérez-Marín, S. García-Cortés, L. R. de Marcos, J. A. Aznárez, and J. A. Méndez, "Self-consistent optical constants of SiC thin films," J. Opt. Soc. Am. A **28**, 2340–2345 (2011).
19. J. I. Larruquert, A. P. Párez-Marín, L. R. d. M. S. García-Cortés, J. A. Aznárez, and J. A. Méndez, "Self-consistent optical constants of sputter-deposited B_4C thin films," J. Opt. Soc. Am. A **29**, 010117–23 (2012).
20. G. Monaco, D. Garoli, R. Frison, V. Mattarello, P. Nicolosi, M. G. Pelizzo, V. Rigato, L. Armelao, A. Giglia, and S. Nannarone, "Optical constants in the EUV Soft x-ray (5–152 nm) spectral range of B_4C thin films deposited by different deposition techniques," in *Proc. SPIE 6317: Advances in X-Ray/EUV Optics, Components, and Applications,* A. M. K. C. Morawe, ed. (SPIE, 2006), p. 631712.
21. R. Soufli, A. L. Aquila, F. Salmassi, M. Fernández-Perea, and E. M. Gullikson, "Optical constants of magnetron-sputtered boron carbide thin films from photoabsorption data in the range 30 to 770 eV," Appl. Opt. **47**, 4633–4639 (2008).
22. D. J. Jones, R. H. French, H. Müllejans, S. Loughin, A. D. Dorneich, and P. F. Carcia, "Optical properties of AlN determined by vacuum ultraviolet spectroscopy and spectroscopic ellipsometry data," J. Mater. Res. **14**, 4337–4344

Optics EXPRESS

(1999).
23. M. Fernández-Perea, M. Vidal-Dasilva, J. I. Larruquert, J. A. Aznárez, J. A. Méndez, E. Gullikson, A. Aquila, and R. Soufli, "Optical constants of evaporation-deposited silicon monoxide films in the 7.1–800 eVphoton energy range," J. Appl. Phys. **105**, 113505 (2009).
24. G. L. Tan, M. F. Lemon, D. J. Jones, and R. H. French, "Optical properties and London dispersion interaction of amorphous and crystalline SiO_2 determined by vacuum ultraviolet spectroscopy and spectroscopic ellipsometry," Phys. Rev. B **72**, 205117 1–10 (2005).
25. A. Singh, M. Sinha, R. K. Gupta, and M. H. Modi, "Optical constants of e-beam-deposited zirconium dioxide measured in the 55–150 Å wavelength region using the reflectivity technique," Appl. Opt. **55**, 3170–3175 (2016).
26. L. R. de Marcos, J. I. Larruquert, J. A. Aznárez, M. Fernández-Perea, R. Soufli, J. A. Méndez, S. L. Baker, and E. M. Gullikson, "Optical constants of SrF_2 thin films in the 25–780 eV spectral range," J. Appl. Phys. **113**, 143501–1–8 (2013).
27. D. Sweeney, "Extreme ultraviolet lithography: Imaging the future," Sci. Technol. Rev. pp. 4–9 (1999).
28. D. Martínez-Garlarce, R. Soufli, D. L. Windt, M. Bruner, E. Gullikson, S. Khatri, E. Spiller, J. C. Robinson, S. Baker, and E. Prast, "Multisegmented, multilayer-coated mirrors for the Solar Ultraviolet Imager," Opt. Eng. **52**, 095102–1–15 (2013).
29. M. W. Zurch, *High-Resolution Extreme Ultraviolet Microscopy: Imaging of Artificial and Biological Specimens with Laser-Driven Ultrafast XUV Sources* (Springer, 2014).
30. T. Ejima, A. Yamazaki, T. Banse, K. Saito, Y. Kondo, S. Ichimaru, and H. Takenaka, "Aging and thermal stability of Mg/SiC and Mg/Y_2O_3 reflection multilayers in the 25–35 nm region," Appl. Opt. **44**, 5446–5453 (2005).
31. W. J. Tropf and M. E. Thomas, "Yttrium oxide (Y_2O_3)," in *Handbook of Optical Constants of Solids,* vol. 2, E. D. Palik, ed. (Academic, 1991).
32. J. Oliver and D. Talbot, "Optimization of deposition uniformity for large-aperture NIF substrates in a planetary rotation system," LLE Rev. **94**, 67–75 (2003). Doe/SF/19460-485.
33. J. Bell, "Thickness uniformity of uranium oxide films sputtered while undergoing planetary motion," (senior thesis, Brigham Young University) (2013). https://cas.byu.edu/cas/login?service=https://www.physics.byu.edu/validate/docs/thesis/344 (Accessed 19 Sept 2017).
34. X. J. Wang, L. D. Zhang, J. P. Zhang, G. He, M. Liu, and L. Q. Zhu, "Effects of post-deposition annealing on the structure and optical properties of Y_2O_3 thin films," Mater. Lett. **62**, 4235–4237 (2008).
35. V. H. Mudavakkat, V. V. Atuchin, V. N. Kruchinin, A. Kayani, and C. V. Ramana, "Structure, morphology and optical properties of nanocrystalline yttrium oxide (Y_2O_3) thin films," Opt. Mater. **34**, 893–900 (2012).
36. P. Lei, J. Zhu, Y. Zhu, C. Jiang, and X. Yin, "Evolution of composition microstructure and optical properties of yttrium oxide thin films with substrate temperature," Surf. Coatings Technol. **229**, 226–230 (2013).
37. C. Ramana, V. H. Mudavakkat, K. K. Bharathi, V. V. Atuchin, and L. D. Pokrovsky, "Enhanced optical constants of nanocrystalline yttrium oxide thin films," Appl. Phys. Lett. **98**, 031905–1–3 (2011).
38. J. Leng, Z. Yu, Y. Li, D. Zhang, X. Liao, and W. Xue, "Optical and electrical properties of Y_2O_3 thin films prepared by ion beam assisted deposition," Appl. Surf. Sci. **256**, 5832–5836 (2010).
39. Y. Nigara, "Measurement of the optical constants of yttrium oxide," Jpn. J. Appl. Phys. **7**, 404–08 (1968).
40. J. Muhlestein, "Optical constants for Y_2O_3 in the extreme ultraviolet," https://www.physics.byu.edu/thesis/archive/2009 (2009). (Accessed 10 Oct 2016).
41. B. D. Smith, "Reflectance measurements of two thin-film materials in the UV," https://www.physics.byu.edu/docs/thesis/693 (2015). (Accessed 13 Dec 2018).
42. E. Gullikson, (private communication, 1999).
43. L. G. Parratt, "Surface studies of solids by total reflection of x-rays," Phys. Rev. **95**, 359 (1954).
44. J. E. Johnson, "Computationally modeling the effects of surface roughness on soft x-ray multilayer reflectors," Master's thesis, Brigham Young University (2006).
45. P. Debye, "Interferenz von röntgenstrahlen und wärmebewegung," Annalen der Physik **348**, 49–92 (1913).
46. G. Acosta, "Scandium oxide thin films and their optical properties in the extreme ultraviole," PhD thesis, Brigham Young University (2007).
47. S. Kimura, F. Arai, and M. Ikezawa, "Optical study on electronic structure of rare-earth sesquioxides," J. Phys. Soc. Jpn. **69**, 3451–3457 (2000).
48. E. Gullikson, "X-ray interactions with matter," http://henke.lbl.gov/optical_constants/mirror2.html. (Accessed 6 July 2018).